Chiral Magnetic Soliton Lattice on a Chiral Helimagnet

Y. Togawa,[1,2] T. Koyama,[3] K. Takayanagi,[1] S. Mori,[2,3] Y. Kousaka,[4] J. Akimitsu,[4] S. Nishihara,[5] K. Inoue,[5,6] A. S. Ovchinnikov,[7] and J. Kishine[8]

[1]N2RC, Osaka Prefecture University, 1-2 Gakuencho, Sakai, Osaka 599-8570, Japan
[2]JST, CREST, Sanbancho, Chiyoda-ku, Tokyo 102-0075, Japan
[3]Department of Materials Science, Osaka Prefecture University, Sakai, Osaka 599-8531, Japan
[4]Department of Physics and Mathematics, Aoyama Gakuin University, Sagamihara, Kanagawa 252-5258, Japan
[5]Department of Chemistry, Faculty of Science, Hiroshima University, Higashi-Hiroshima, Hiroshima 739-8526, Japan
[6]IAMR, Facility of Science, Hiroshima University, Higashi-Hiroshima, Hiroshima 739-8530, Japan
[7]Department of Physics, Ural Federal University, Ekaterinburg, 620083, Russia
[8]Department of Basic Sciences, Kyushu Institute of Technology, Kitakyushu, 804-8550, Japan

(Received 16 October 2011; published 5 March 2012)

Using Lorenz microscopy and small-angle electron diffraction, we directly present that the chiral magnetic soliton lattice (CSL) continuously evolves from a chiral helimagnetic structure in small magnetic fields in $Cr_{1/3}NbS_2$. An incommensurate CSL undergoes a phase transition to a commensurate ferromagnetic state at the critical field strength. The period of a CSL, which exerts an effective potential for itinerant spins, is tuned by simply changing the field strength. Chiral magnetic orders observed do not exhibit any structural dislocation, indicating their high stability and robustness in $Cr_{1/3}NbS_2$.

DOI: 10.1103/PhysRevLett.108.107202 PACS numbers: 75.25.−j, 61.05.J−, 68.37.Lp, 75.50.Cc

The concept of chirality, meaning left- or right-handedness, plays an essential role in the symmetry properties of nature at all length scales from elementary particles to biological systems [1]. In materials science, chiral materials are frequently found in molecules or crystals with helical structures, which break mirror and inversion symmetries but combine rotational and translational symmetries. Chiral structure sometimes leads to the emergence of intriguing functionalities such as a tunable optical response in chiral nematic liquid crystals [2]. These phenomena occur because electrons distribute themselves along the chiral framework of atomic configurations and their rotational and translational motions couple to give specific physical processes.

In magnetic crystals belonging to chiral space group such as MnSi [3], $Fe_{1-x}Co_xSi$ [4], $Cr_{1/3}NbS_2$ [5], $CsCuCl_3$ [6] and molecule-based magnets [7], orbital motions of localized electrons with spin magnetic moments take helical paths in the chiral framework of atoms and mediate coupling of the neighboring spins of electrons via the relativistic spin-orbit interaction called Dzyaloshinskii-Moriya (DM) interaction [8,9].

In this Letter, we demonstrate an emergence of periodic and nonlinear magnetic order called chiral magnetic soliton lattice (CSL) [10–12] in addition to harmonic (linear) magnetic order of chiral helimagnetic structure (CHM) in chiral magnetic crystals of $Cr_{1/3}NbS_2$ by means of Lorenz microscopy [13,14] and small-angle electron diffraction (SAED) [15,16]. We have directly observed that upon applying small magnetic fields perpendicular to the helical axis, CHM with 48 nm period continuously turns into CSL, which consists of forced FM domains periodically partitioned by 360° domain walls. Incommensurate CSL undergoes a continuous phase transition to commensurate FM state at the critical field strength. Applying magnetic field causes continuous growth of the period of CSL from 48 nm toward infinity at the incommensurate-to-commensurate (I-C) phase transition. Hence, the effective magnetic superlattice potential for the itinerant quantum spins can be tuned by simply changing the field strength. The chiralities of CHM and CSL are identified to be left handed in the present crystals. CHM and CSL appear regularly and present no structural dislocation in all regions of the specimens examined irrespective of scratched defects fabricated by focused gallium-ion beams (FIB), indicating that CHM and CSL are macroscopic order of spin magnetic moments and, surprisingly, obtain high stability and robustness against perturbation in $Cr_{1/3}NbS_2$. These specific features of CHM and CSL are probably because CHM and CSL are macroscopically induced by the uniaxial DM interaction that is allowed in $Cr_{1/3}NbS_2$ hexagonal crystals belonging to noncentrosymmetric chiral space group. Present observations will be the first step to explore a variety of functionality [17–20] of CHM and CSL in chiral magnetic crystals for spintronic device applications.

$Cr_{1/3}NbS_2$ has a layered hexagonal structure of 2H-type NbS_2 intercalated by Cr atoms which belongs to the space group $P6_322$ as shown in Fig. 1(a). Studies of $Cr_{1/3}NbS_2$ were started in the early 1970s when chemical vapor transport method was used to grow $Cr_{1/3}NbS_2$ single crystals [21]. Cr atoms are in the trivalent state and have localized electrons with spins of $S = 3/2$, whereas conduction electrons are in an unfilled band originated from Nb atoms. Crystals with structural chirality allow the

 © 2012 American Physical Society

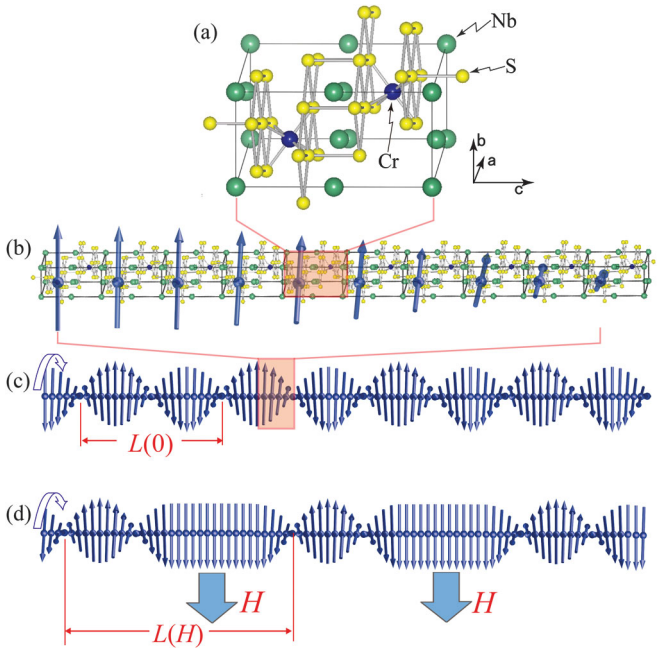

FIG. 1 (color). Schematic diagram of crystalline and magnetic structures of $Cr_{1/3}NbS_2$. (a) A unit cell of the crystal. Spin magnetic moments of localized electrons rotate in the ab plane along the helical c axis because of DM interaction, giving rise to CHM. A part of left-handed CHM is schematically drawn in ten unit cells in (b), whereas a whole left-handed CHM in (c). (d) In magnetic fields perpendicular to the helical c axis, CHM continuously transforms into CSL. CSL has the same magnetic chirality as the underlying CHM.

monoaxial DM interaction in the form of $-\boldsymbol{D}\cdot\boldsymbol{S}_1\times\boldsymbol{S}_2$ between localized neighboring spins $\boldsymbol{S}_1$ and $\boldsymbol{S}_2$ along the crystallographic c axis in $Cr_{1/3}NbS_2$. Here, $\boldsymbol{D}$ represents the DM vector. Competition between DM interaction and the isotropic ferromagnetic (FM) coupling ($J>0$) gives rise to the helical structure of spin magnetic moments $\boldsymbol{S}(z)=S(\cos\phi(z),\sin\phi(z),0)$ with the azimuthal angle given by $\phi(z)=Q_0 z$, as shown in Figs. 1(b) and 1(c). z is defined as a coordinate along the helical axis (c axis) and Q_0 is the single modulation wave number of the helix given by $Q_0=a_0^{-1}\tan^{-1}(D/J)$ with a_0 being the atomic lattice constant along the helical axis (1.21 nm in $Cr_{1/3}NbS_2$ [21]). Importantly, the direction of $\boldsymbol{D}$ determines whether spin magnetic moments rotate in a left- or right-handed manner along the helical axis, thus providing chirality to the given magnetic helix and calling it CHM. The magnitude of $D=|\boldsymbol{D}|$ is usually 1 or 2 orders of magnitude smaller than J because of its relativistic origin. Therefore, a spatial period of CHM, $L(0)=2\pi/Q_0\cong 2\pi a_0 J/D$ amounts to some tens of nanometers in chiral magnetic crystals, which is obviously incommensurate with respect to the background atomic lattice.

Under magnetic fields applied perpendicular to the helical axis, the magnetic field favors FM domains commensurate to the atomic lattice because of Zeeman energy while the DM interaction tries to keep incommensurate CHM. This situation is well reproduced by the effective one-dimensional chiral sine-Gordon model [10–12,17–20]. Consequently, the order of CHM is periodically distorted and CSL appears as the ground state unique to chiral magnetic crystals in the magnetic field as shown in Fig. 1(d). CSL is the nonlinear magnetic superlattice consisting of forced FM domains periodically partitioned by 360° magnetic domain walls. The period of CSL is given by $L(H)=8K(\kappa)E(\kappa)/(\pi Q_0)$ [10–12,17–20], where $K(\kappa)$ and $E(\kappa)$, respectively, denote the elliptic integrals of the first and second kinds with the elliptic modulus κ ($0\le\kappa\le 1$). The modulus κ is determined by minimizing the CSL formation energy and given by $\kappa/E(\kappa)=\sqrt{H/H_c}$, where $H_c=(\pi a_0 Q_0/4)^2 JS$ corresponds to $\kappa=1$. $\kappa/E(\kappa)$ monotonically increases from 0 to 1 as κ changes from 0 to 1. Then, H_c has a meaning of the critical field strength at which the continuous phase transition from CSL at $H<H_c$ to the commensurate forced FM states state at $H>H_c$ occurs. Using the relations $K(0)=E(0)=\pi/2$, we see that the dimensionless ratio $L(H)/L(0)$ given by

$$L(H)/L(0)=4K(\kappa)E(\kappa)/\pi^2, \tag{1}$$

which depends solely on H/H_c. As H/H_c increases, $L(H)/L(0)$ evolves monotonically toward infinity at $H/H_c=1$.

Magnetic structure of $Cr_{1/3}NbS_2$ was first investigated experimentally by small-angle neutron diffraction at zero magnetic field [21]. Below the Curie temperature $T_C=127$ K, $Cr_{1/3}NbS_2$ exhibits a magnetic Bragg peak of 0.13 nm^{-1}, which was considered as a manifestation of helical order with magnetic moments rotating in the ab plane in a 48 nm period along the c axis.

In the meanwhile, a steep change of magnetization at H_c applied perpendicular to the helical axis was interpreted as the discontinuous phase transition between CHM and forced FM states [5,21]. However, an intermediate phase in perpendicular fields below H_c was not identified as CSL state.

The transition at H_c should be interpreted as the continuous I-C phase transition theoretically envisioned by Dzyaloshinskii [10]. This type of transition was actually reported to occur in $Ba_2CuGe_2O_7$ [22]. Recently, we reexamined magnetization profiles of $Cr_{1/3}NbS_2$ and found that the data indirectly suggest a formation of CHM and CSL [12,23].

Previous theoretical treatments demonstrate that CSL will support a variety of interesting functions for spintronic applications in magnetic chiral crystals. CSL enables us to carry magnetic information [17] and exhibits characteristic physical properties such as magnetic-phonon-like elementary excitations [18], current-driven sliding motion [19], and field-induced metal-to-insulator transition [20]. Therefore, direct observations of CSL have been eagerly desired in the magnetic system.

There were several reports on real-space imaging of a helical magnetic structure in cubic crystals of $Fe_{0.5}Co_{0.5}Si$ [24] and FeGe [25] in $P2_13$ chiral space group by means of Lorentz microscopy using a transmission electron microscope (TEM). It should be noted that Lorentz microscopy, in principle, detects solely an in-plane component of magnetic moments in the specimen. Thus, additional experimental methods will be required to analyze real-space images by Lorentz microscopy [26] and specify a detailed magnetic structure of CHM and CSL.

To obtain direct evidence of CHM and CSL formation, we have performed Lorentz microscopy [13,14] and SAED [15,16] in $Cr_{1/3}NbS_2$. Figure 2(a) shows an example of Lorentz micrographs in 0 T at 110 K. Thin specimens, typically of 5 μm in width, 13 μm in length, and 70 nm in thickness, are fabricated for TEM observations by using FIB. Lines patterned with bright and dark contrast are repeatedly found perpendicular to the c axis in almost all the regions of the specimen. The contrast alternately changes in a nearly sinusoidal manner with 46 nm period in a line profile of the contrast intensity in Fig. 2(b). This sinusoidal pattern of in-plane magnetic moments is observed in a series of Lorentz micrographs taken at various defocus values less than 8 μm and reverses the contrast when defocusing oppositely.

Details of sinusoidal magnetic pattern are precisely examined in the reciprocal space by using SAED. When electron waves pass through magnetic fields or magnetization, they are deflected, change the phase, and form characteristic patterns of magnetic electron diffraction. It has been established that periodic magnetic structures like stripe magnetic domains act as phase gratings of electron waves, which produces an electron diffraction pattern of regularly spaced spots [15,16]. To be exact, multiple diffraction spots appear due to higher harmonic orders that the stripe magnetic domains contain. In our problem, CHM consists of the harmonic (sinusoidal) modulation of magnetic moments with the single wave vector Q_0, thus providing magnetic diffraction spots at $\pm Q_0$. Figures 2(c) and 2(d) explicitly present expected behavior for CHM; a pair of diffraction spots of $(48\ \mathrm{nm})^{-1}$ along the c axis are clearly found close to 000 and 001 diffraction spots, which is well accorded with the data obtained by real-space Lorentz images in Fig. 2(b) and small-angle neutron diffraction [21].

Furthermore, the harmonic modulation of in-plane magnetic moments in CHM contributes a fine change of the shape of the central spot of SAED since electron waves are deflected by Lorentz force in a sinusoidal manner in CHM. This is a similar analogy with magnetic electron diffraction of a 180° Bloch-type domain wall, in which the central spot is split into two symmetric spots with diffusive streak between the two spots [13,16]. In Fig. 2(e), an ellipsoidal shape of the central spot is observed along the c axis in SAED taken at very long camera length of 300 m [16]. The size of the central spot is about 7.4×10^{-6} rad along the c axis, giving 0.086 T for the saturation magnetization in TEM specimens with 70 nm thickness. This estimated value is in good agreement with 0.0862 T ($1.5\mu_B$/Cr atom; μ_B is Bohr's magneton) at 110 K obtained by magnetization measurements of the same specimens [23]. Therefore, our data in SAED and real-space Lorentz micrographs explicitly identify the existence of CHM in

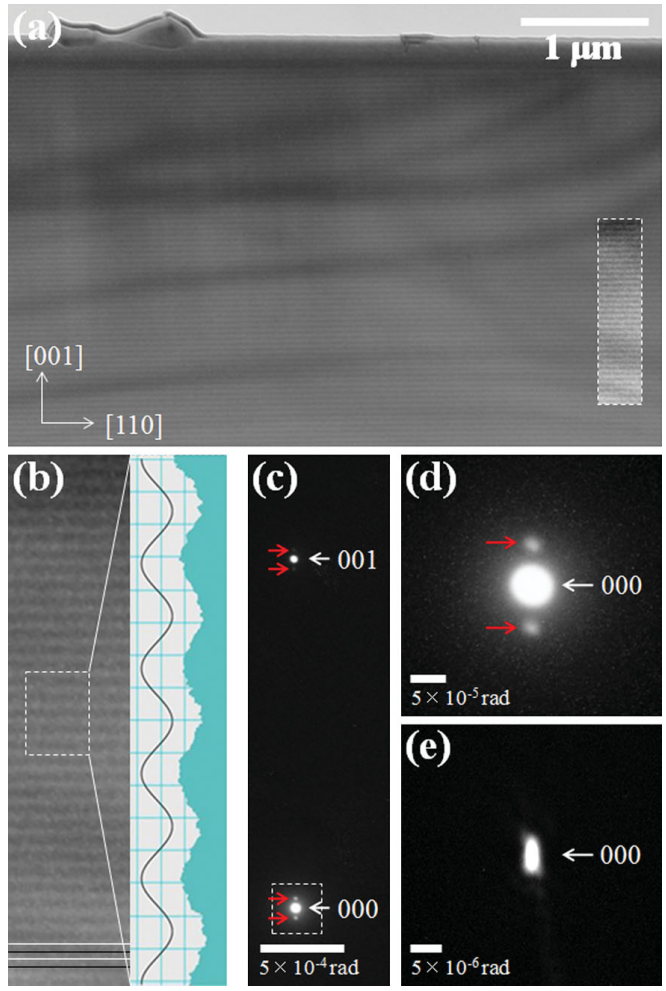

FIG. 2 (color). Underfocused Lorentz micrographs and SAEDs of CHM in $Cr_{1/3}NbS_2$ in 0 T at 110 K. (a) Defocus value is 512 nm. Wide curved dark fringes are bend contours. A broken square area, in which the contrast is enhanced, corresponds to a field of view in (b). (b) Enlarged lines pattern of CHM together with a line profile of the contrast intensity integrated in a dotted square region. White and black solid lines are guides to the eye. Vertical grid spacing corresponds to 15 nm. The period is estimated to be 46 nm. (c) and (d) SAEDs performed at camera length (CL) of 30 m. Electron diffraction spots 000 and 001 in (c) give the spatial frequency of $(1.2\ \mathrm{nm})^{-1}$ in the reciprocal space. CHM provides magnetic satellite spots with the spatial frequency of $(48\ \mathrm{nm})^{-1}$ close to 000 and 001 indicated by red arrows. (e) An ellipsoidal shape of the central spot of SAED taken at 300 m CL by using electron waves with a divergence angle of 6×10^{-7} rad.

$Cr_{1/3}NbS_2$, while the chirality of CHM is discussed in the following paragraphs.

Next, let us examine how CHM turns into CSL in magnetic fields perpendicular to the helical c axis. Figure 3 shows that sinusoidal pattern of CHM transforms into another periodic pattern segmented by contrast lines, which is ascribed to CSL. Importantly, line profile of the contrast intensity in Fig. 3(d) presents that the periodic pattern is partitioned by three contrast lines, namely, central dark contrast line accompanied with two adjacent bright contrast lines.

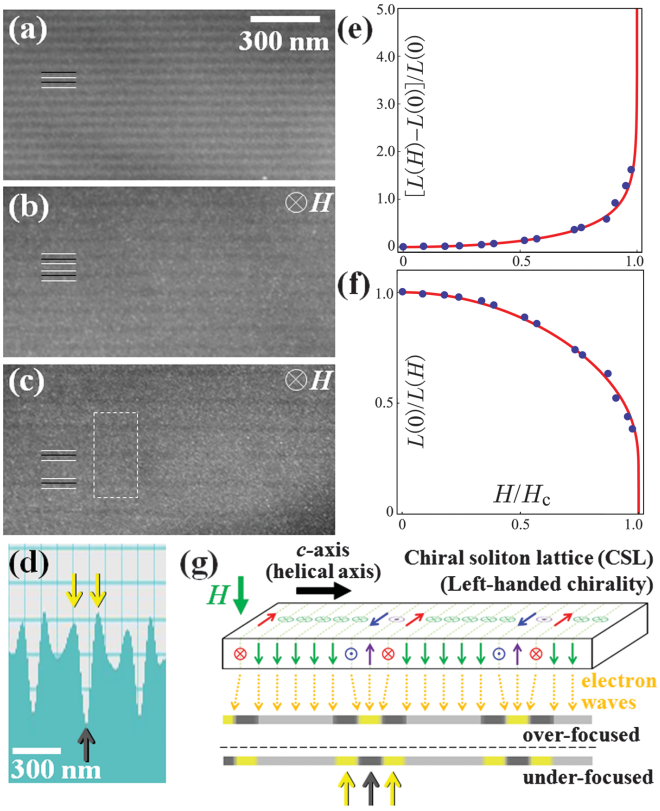

FIG. 3 (color). Underfocused Lorentz micrographs at 110 K in 0 T (a) and perpendicular magnetic fields of 0.208 T (b) and 0.224 T (c). Defocus value is 900 nm. (d) Line profile of the contrast intensity integrated in a dotted square in (c). (e) Experimental plot of $\Delta L(H)/L(0) = [L(H) - L(0)]/L(0)$ with fitting curve being given by Eq. (1). H_c and $L(0)$ are experimentally determined as ~0.230 T and 48 nm, respectively. (f) Experimental plot of the soliton density $L(0)/L(H)$ which plays a role of the order parameter of the I-C phase transition. (g) CSL deflects electron waves and forms characteristic contrast patterns in Lorentz micrographs depending on the magnetic chirality. Note that the contrast reverses when defocusing in the opposite direction. In the case of left-handed CSL, when electron waves pass through 360° magnetic domain walls in CSL, they are converged and virtually diverged in over- and underfocused micrographs, respectively. This action of left-handed (right-handed) CSL on electron waves in the overfocused condition is similar to the convex (concave) cylindrical lenses effect, which enables us to recognize the chirality of CSL or CHM.

In Fig. 3(e), we show the experimental plot of $\Delta L(H)/L(0)$. It is seen that upon increasing H, the period of CSL evolves monotonically and finally diverges at $H_c \sim 0.230$ T. This behavior is consistent with theoretical scenario based on the CSL formation. Actually, as can be seen in Fig. 3(e), the experimental data are well fitted by using a single function given by Eq. (1). Above H_c, no periodic pattern due to CSL is observed in Lorentz micrographs, indicating that the system undergoes the I-C phase transition from CSL to forced FM state. In the I-C phase transition described by the chiral sine-Gordon model, the soliton density $L(0)/L(H)$ plays a role of the order parameter. To make clear this point, we show the plot of $L(0)/L(H)$ in Fig. 3(f).

In perpendicular magnetic fields, forced FM domains in CSL and forced FM state have out-of-plane magnetic moments toward the applied magnetic field. In the present experimental configuration, they are parallel to the propagation direction of electron waves, thus not providing any characteristic contrast in Lorenz micrographs. On the other hand, magnetic boundaries of CSL, i.e., 360° magnetic domain walls are identified by the presence of three lines with bright and dark contrast because electron waves sense oppositely oriented components of in-plane magnetic moments in 360° domain walls.

At the same time, the chirality of CSL can be uniquely determined by the sequence of contrast lines: dark-bright-dark or bright-dark-bright. In downward perpendicular magnetic field, CSL with left-handed (right-handed) chirality gives rise to a single dark (bright) contrast line with two adjacent bright (dark) contrast lines in underfocused Lorenz micrographs, as schematically drawn in Fig. 3(g). Therefore, the chirality of CSL is revealed to be left handed in the present crystals, as recognized in Fig. 3(d). Moreover, it can be safely noted that the chirality of CHM is also left-handed since CSL develops from CHM and inherits the same magnetic chirality.

Remarkably enough, CHM and CSL are very straight perpendicular to the helical axis and appear almost all over the specimen as partially shown in Figs. 2 and 3. In addition, CHM and CSL present no structural dislocation and persist against crystal defects that potentially exist in specimens and scratch defects extrinsically made by an irradiation of FIB along [001] direction during TEM specimen fabrication. Specific features of high stability and robustness might be originated from the fact that both CHM and CSL are manifestations of the macroscopic order of spin magnetic moments. Indeed, the chiral magnetic orders are macroscopically induced in $Cr_{1/3}NbS_2$ by the DM interaction that is allowed in the system because the hexagonal crystal of $Cr_{1/3}NbS_2$ belongs to noncentrosymmetric chiral space group.

Fine, stable, robust, and tunable chiral magnetic orders can be utilized to construct nanoscaled magnetic structures over macroscopic scales. Controlling their behavior will be

of great significance in nanomagnetism and spintronics. Particularly, chiral magnetic orders in $Cr_{1/3}NbS_2$ work as tunable effective potential for itinerant spins [20]. The present finding of chiral magnetic orders opens a door to exploring fascinating functionality [17–20] and to elaborating a new paradigm for spintronics applications based on chiral magnetic crystals.

[1] G. H. Wagniere, *On Chirality and the Universal Asymmetry* (Wiley-VCH, Zurich, Weinheim, 2007).
[2] H. J. Coles and M. N. Pivnenko, Nature (London) **436**, 997 (2005).
[3] Y. Ishikawa, K. Tajima, D. Bloch, and M. Roth, Solid State Commun. **19**, 525 (1976).
[4] S. V. Grigoriev *et al.*, Phys. Rev. Lett. **102**, 037204 (2009).
[5] T. Moriya and T. Miyadai, Solid State Commun. **42**, 209 (1982).
[6] Y. Kousaka *et al.*, J. Phys. Soc. Jpn. **78**, 123601 (2009).
[7] K. Inoue *et al.*, Angew. Chem., Int. Ed. **42**, 4810 (2003).
[8] I. E. Dzyaloshinskii, J. Phys. Chem. Solids **4**, 241 (1958).
[9] T. Moriya, Phys. Rev. **120**, 91 (1960).
[10] I. E. Dzyaloshinskii, Sov. Phys. JETP **19**, 960 (1964).
[11] Y. A. Izyumov, Sov. Phys. Usp. **27**, 845 (1984).
[12] J. Kishine, K. Inoue, and Y. Yoshida, Prog. Theor. Phys. Suppl. **159**, 82 (2005).
[13] P. J. Grundy and R. S. Tebble, Adv. Phys. **17**, 153 (1968).
[14] Y. Togawa *et al.*, Phys. Rev. Lett. **95**, 087002 (2005).
[15] M. J. Goringe and J. P. Jakubovics, Philos. Mag. **15**, 393 (1967); R. H. Wade, Phys. Status Solidi (b) **19**, 847 (1967).
[16] T. Koyama, Y. Togawa, K. Takenaka, and S. Mori, J. Appl. Phys. (to be published).
[17] I. G. Bostrem, J. Kishine, and A. S. Ovchinnikov, Phys. Rev. B **78**, 064425 (2008); A. B. Borisov, J. Kishine, I. G. Bostrem, and A. S. Ovchinnikov, Phys. Rev. B **79**, 134436 (2009).
[18] J. Kishine and A. S. Ovchinnikov, Phys. Rev. B **79**, 220405 (R) (2009).
[19] J. Kishine, A. S. Ovchinnikov, and I. V. Proskurin, Phys. Rev. B **82**, 064407 (2010).
[20] J. Kishine, I. V. Proskurin, and A. S. Ovchinnikov, Phys. Rev. Lett. **107**, 017205 (2011).
[21] T. Miyadai *et al.*, J. Phys. Soc. Jpn. **52**, 1394 (1983).
[22] A. Zheludev *et al.*, Phys. Rev. Lett. **78**, 4857 (1997).
[23] Y. Kousaka *et al.*, Nucl. Instrum. Methods Phys. Res., Sect. A **600**, 250 (2009).
[24] M. Uchida *et al.*, Science **311**, 359 (2006).
[25] M. Uchida *et al.*, Phys. Rev. B **77**, 184402 (2008).
[26] F. Nori and A. Tonomura, Science **311**, 344 (2006).